

Effect of the 2022 summer drought across forest types in Europe

Mana Gharun¹, Ankit Shekhar^{2,3}, Jingfeng Xiao⁴, Xing Li⁵, Nina Buchmann²

¹ Institute of Landscape Ecology, University of Münster, Münster, Germany

² Institute of Agricultural Sciences, ETH Zürich, Zürich, Switzerland

³ Agricultural and Food Engineering Department, Indian Institute of Technology Kharagpur, Kharagpur, India

⁴ Earth Systems Research Center, University of New Hampshire, New Hampshire, USA

⁵ Research Institute of Agriculture and Life Sciences, Seoul National University, Seoul, South Korea

Correspondence to: Mana Gharun, mana.gharun@uni-muenster.de

Abstract

Forests in Europe experienced record-breaking dry conditions during the 2022 summer. The direction in which various forest types respond to climate extremes during their growing season is contingent upon an array of internal and external factors. These factors include the extent and severity of the extreme conditions and the tree ecophysiological characteristics adapted to environmental cues, which exhibit significant regional variations. In this study we aimed to: 1) quantify the extent and severity of the extreme soil and atmospheric dryness in 2022 in comparison to two most extreme years in the past (2003 and 2018), 2) quantify response of different forest types to atmospheric and soil dryness in terms of canopy browning and photosynthesis, and 3) relate the functional characteristics of the forests to the emerging responses observed remotely at the canopy level. For this purpose, we used spatial meteorological datasets between 1970 to 2022 to identify conditions with extreme soil and atmospheric dryness. We used the near-infrared reflectance of vegetation (NIRv) derived from the MOderate Resolution Imaging Spectroradiometer (MODIS), and the OCO-2 solar induced fluorescence (GOSIF) as an observational proxy for ecosystem gross productivity, to quantify the response of forests at the canopy level.

30 In summer 2022, southern regions of Europe experienced exceptionally pronounced
31 atmospheric and soil dryness. These extreme conditions resulted in a 30% more
32 widespread decline in GOSIF across forests compared to the drought of 2018, and 60%
33 more widespread decline compared to the drought of 2003. Although the atmospheric
34 and soil drought were more extensive and severe (indicated by a larger observed
35 maximum z-score) in 2018 compared to 2022, the negative impact on forests, as
36 indicated by declined GOSIF, was significantly larger in 2022. Different forest types were
37 affected in varying degrees by the extreme conditions in 2022. Deciduous broad-leaved
38 forests were the most negatively impacted due to the extent and severity of the drought
39 within their distribution range. In contrast, areas dominated by Evergreen Needle-Leaf
40 Forests (ENF) in northern Europe experienced a positive soil moisture (SM) anomaly and
41 minimal negative vapor pressure deficit (VPD) in 2022. These conditions led to enhanced
42 canopy greening and stronger solar-induced fluorescence (SIF) signals, benefiting from
43 the warming. The higher degree of canopy damage in 2022, despite less extreme
44 conditions, highlights the evident vulnerability of European forests to future droughts.

45

46 *Keywords: photosynthesis, soil drought, atmospheric drought, canopy browning, gross*
47 *primary production*

48 **Introduction**

49 The frequency and intensity of drought events have been rising globally, and future global
50 warming is expected to further increase their occurrence (Seneviratne et al. 2021;
51 Röthlisberger and Papritz 2023). Particularly over the past two decades, many regions in
52 Europe have experienced widespread drought conditions, notably during the summers of
53 2003, 2010, and 2018 (Bastos et al. 2020; Zhou et al. 2023). The extreme conditions
54 caused widespread ecological disturbances (Müller and Bahn 2022) and reduced the
55 capacity of forests for carbon uptake, thereby diminishing their potential for mitigating
56 climate change (van der Woude et al. 2023). Additionally, heatwaves and prolonged
57 droughts stress vegetation, making it more susceptible to other biotic and abiotic stress
58 factors. This increased vulnerability leads to higher tree mortality, elevated wildfire risks,

59 and a loss of biodiversity among plants and animals living at the edge of their temperature
60 tolerance. These conditions also alter phenology and plant development, causing
61 cascading effects on ecosystem functioning (Seidl et al. 2017).

62 The spatial extent and severity of drought events vary, and their impacts depend on local
63 ecological characteristics of the forests, species-specific temperature and moisture
64 thresholds that limit tree functioning, as well as adaptation strategies and acclimation of
65 trees to more frequent and intense extreme conditions (Gessler et al. 2020). For example,
66 comparing the 2003 and 2018 extreme years, the year 2018 was characterized by a
67 climatic dipole, featuring extremely hot and dry weather conditions north of the Alps but
68 comparably cool and moist conditions across large parts of the Mediterranean. Negative
69 drought impacts appeared to affect an area 1.5 times larger and to be significantly
70 stronger in summer 2018 compared to summer 2003 (Buras et al. 2020).

71 In 2022, Europe faced its second hottest and driest year on record, with the summer of
72 that year being the warmest summer ever recorded. Conditions in summer 2022 led to
73 record-breaking heatwave and drought events across many regions (Copernicus Climate
74 Change Service, 2023). Compound drought and heatwave conditions in 2022 caused
75 widespread crop damage, water shortages, and wildfires across Europe. The hardest-hit
76 areas were the Iberian Peninsula, France, and Italy, where temperatures exceeded 2.5°C
77 above normal, and severe droughts persisted from May to August (Tripathy and Mishra
78 2023). The reduced soil moisture due to precipitation deficits and high temperatures,
79 contributed to the persistence and severity of drought, creating a positive feedback loop
80 where dry soils led to even drier conditions (Tripathy and Mishra 2023).

81 Drought and heatwaves have a range of detrimental effects on trees and forests. The
82 most immediate impact is that elevated air temperatures and increased dryness, whether
83 in the soil or in the atmosphere, disrupt mesophyll and stomatal conductance, thereby
84 impairing carbon uptake (Marchin et al. 2022). Plants reduce stomatal conductance under
85 severe drought to reduce water stress at the expense of reduced rates of photosynthesis
86 (Oren et al., 1999). Drought also increases the chance of hydraulic failure, which can lead
87 to tree mortality (Choat et al. 2018). Additionally, rising temperatures reduce the
88 enzymatic activity in trees, which in turn diminishes the forest's gross primary productivity
89 (Gourlez de la Motte et al. 2020). Elevated temperatures can also increase respiration

90 rates in both soil and trees, which reduces the forest's net carbon uptake and their ability
91 to mitigate anthropogenic CO₂ emissions (van der Molen et al. 2011; Anjileli et al. 2021).
92 Drought also restricts the movement of nutrients in soil water, reducing their availability
93 to trees and consequently impacting their growth and productivity (Bauke et al. 2022).
94 Changes in plant water-use and nutrient cycling can trigger feedback loops that magnify
95 the effects of drought and heat stress. For instance, reduced plant cover can increase
96 soil temperatures and further accelerate water loss and increase plant water demand
97 (Haesen et al. 2023). On the other hand, increased atmospheric dryness or reduced soil
98 moisture levels increase stomatal closure which limits transpiration and leads to higher
99 leaf temperature that intensifies heat stress on plants (Drake et al. 2018). Reduced
100 transpiration and photosynthesis elevate surface temperatures and atmospheric CO₂
101 concentrations, altering local and regional climate patterns and intensifying the frequency
102 and severity of extreme events (Humphrey et al. 2018). These effects vary significantly
103 depending on forest type and species composition. Together with the characteristics of
104 the extreme events themselves – such as their extent and severity- this variability
105 complicates our understanding of how drought affects the functionality of different forest
106 ecosystems (Gharun et al. 2020; Shekhar et al. 2023). These feedback loops highlight
107 the urgent need to assess how climate extremes impact different forest types, which are
108 crucial for sequestering significant portions of anthropogenic emissions. Our study aims
109 to 1) quantify the extent and severity of the extreme conditions in 2022 – focusing on soil
110 and atmospheric dryness- and compare them to those of two previous extreme years
111 (2003, 2018), 2) quantify the responses of different forest types to drought in terms of
112 canopy browning and photosynthesis, and 3) connect the functional characteristics of the
113 forests with the canopy-level responses observed.

114 **Methods**

115 *Meteorological dataset*

116 We used Europe-wide gridded datasets covering daily mean air temperature (T_{air}; °C),
117 daily mean relative humidity (RH; %) and daily mean soil moisture (SM; m³m⁻³) for the
118 topsoil layer (0-7 cm depth), spanning from 2000-2022. The study area encompasses

119 longitudes from 11°W to 32°E, and latitudes from 35.8°N to 72°N, approximately 4.45
120 million km². We sourced the Tair and RH datasets from the E-OBS v27.0e dataset which
121 provides daily data at 0.1°×0.1° spatial resolution (Cornes et al., 2018; Klein et al., 2002).
122 We calculated daily mean vapor pressure deficit (VPD; kPa) from Tair and RH using
123 Equation 1 (Dee et al. 2011).

124

$$125 \quad VPD = \left(1 - \frac{RH}{100}\right) \times 0.6107 \times 10^{\frac{7.5 \times T_{air}}{237.3 + T_{air}}} \quad (1)$$

126

127 The SM dataset was extracted from the most recent reanalysis data from ECMWF's
128 (European Centre for Medium-range Weather Forecasts) new land component of the fifth
129 generation of European Reanalysis (ERA5-Land) dataset (daily at 0.1°×0.1° resolution;
130 Munoz-Sabater et al., 2021). ERA5-Land provides soil moisture (SM) data at an hourly
131 interval with a spatial resolution of 0.1° × 0.1°. For our analysis, we aggregated the hourly
132 SM data into daily averages. Recent validation studies using in-situ measurements and
133 satellite data have confirmed the high accuracy of surface SM simulations from ERA5-
134 Land (Albergel et al., 2012; Lal et al., 2022; Muñoz-Sabater et al., 2021). Additionally, SM
135 data from ERA5-Land have been utilized to investigate drought and global SM patterns
136 (see Lal et al., 2023; Shekhar et al., 2024b). We re-sampled the Tair, VPD, and SM data
137 from daily (0.1° × 0.1°) to 8-day (0.05° × 0.05°) intervals to align with the temporal and
138 spatial resolution of the vegetation response dataset.

139 *Forest canopy response dataset*

140 In order to assess the forest canopy response to drought stress, we used two satellite-
141 based proxies:

142 1) The structure-based NIRv (near-infrared of vegetation index derived from MODIS
143 (Moderate Resolution Imaging Spectroradiometer; 8-day 500m x 500m MOD09Q1 v6.1
144 product) which is calculated using surface spectral reflectance at near-infrared band
145 (RNIR) and red band (RRed) as shown in Equation 2 (Badgley et al. 2017). The calculated
146 NIRv at 500m resolution was aggregated to a 0.05°×0.05° resolution (daily) by averaging.

147

148
$$NIR_V = R_{NIR} \times \frac{R_{NIR} - R_{Red}}{R_{NIR} + R_{Red}} \quad (2)$$

149

150 2) The physiological-based reconstructed global OCO-2 (Observation Carbon
151 Observatory - 2) solar induced fluorescence (GOSIF) dataset. Solar-induced
152 fluorescence (SIF) is an energy flux (unit: $Wm^{-2}\mu m.sr^{-1}$) reemitted as fluorescence by the
153 chlorophyll *a* molecules in the plants (Baker, 2008). Recent extensive research has
154 established a strong link between Solar-Induced Fluorescence (SIF) and vegetation
155 photosynthesis, validating SIF as an effective proxy for ecosystem gross primary
156 productivity (GPP) (Li et al. 2018; Magney et al. 2019; Shekhar et al., 2022). The GOSIF
157 dataset was created by training a Cubist Regression Tree model to gap-fill SIF retrievals
158 from OCO-2 satellite. This was done using MODIS Enhanced Vegetation Index (EVI) and
159 meteorological reanalysis data from MERRA-2 (Modern-Era Retrospective analysis for
160 Research and Applications), which includes photosynthetically active radiation (PAR),
161 VPD, and air temperature (see Li and Xiao, 2019). We downloaded GOSIF data set (v2)
162 from the Global Ecology Data Repository
163 (http://data.globalecology.unh.edu/data/GOSIF_v2/, last accessed on 25 July 2024). The
164 GOSIF was available from 2000-2022 at 8-day temporal scale with a spatial resolution of
165 $0.05^{\circ} \times 0.05^{\circ}$ (Li and Xiao, 2019).

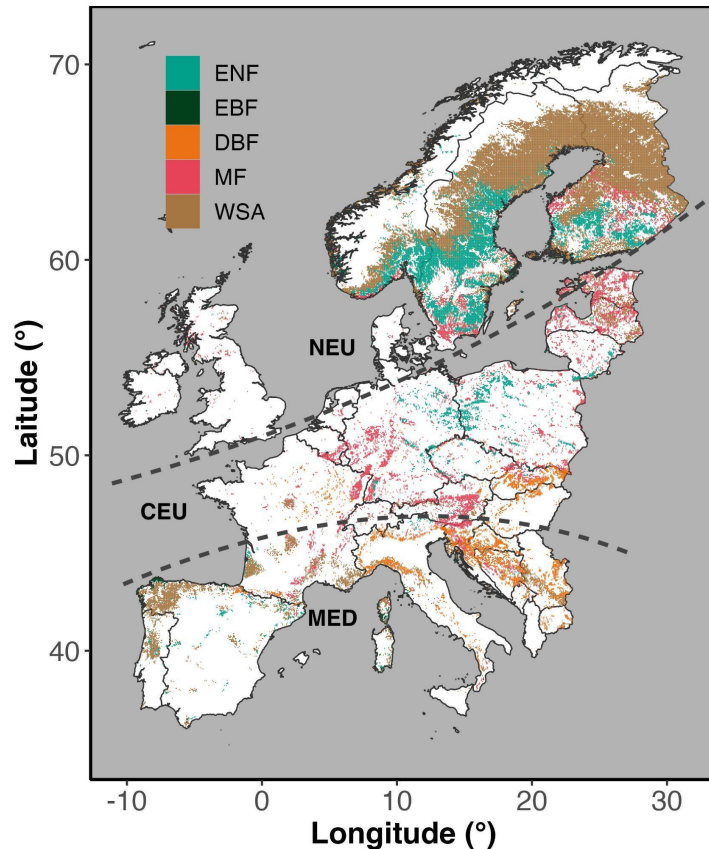
166 GOSIF signals provide information about physiological response of forest photosynthesis
167 while NIR_v (a recently developed vegetation index) signals provide information about the
168 health status of the canopy. NIR_v is preferred over NDVI and EVI as it can isolate the
169 vegetation signal, mitigate mixed-pixel issue, and partly address the influences of
170 background brightness and soil contamination (Zhang et al. 2022). The two vegetation
171 proxies used in this study are anticipated to offer complementary insights into vegetation
172 response to drought.

173 *Land cover dataset*

174 In this study, we focused on five different types of forests (and woodlands) across Europe,
175 namely, evergreen needleleaf forest (ENF), evergreen broadleaf forest (EBF), deciduous
176 broadleaf forest (DBF), mixed forest (MF), and woody savannas (WSA). The spatial

177 distribution of the five different forest types across Europe is shown in Figure 1. We used
178 the yearly MODIS land cover product (MCD12C1 version 6.1 at $0.05^{\circ} \times 0.05^{\circ}$ resolution)
179 for the years of 2001, 2006, 2011, 2016 and 2021, to extract total areas covered by each
180 forest type. Area of each grid cell was calculated using trigonometric equations
181 considering the latitudinal and longitudinal variations arising due to Earth's spherical
182 shape (Ellipsoid). Only areas that were consistently identified as each forest type over the
183 five-year period were included in the analysis. This means that only pixels common
184 across these five years were selected, and with more than 50% of the $0.05^{\circ} \times 0.05^{\circ}$ pixel
185 area identified as forests. The forested areas selected for this study encompassed
186 907,875 km², which represents approximately 24% of Europe's total land area. Out of the
187 total area about 23% (206'212 km²) was dominated by ENFs distributed largely across
188 Northern Europe (NEU). Approximately 1% (7'000 km²) of the area was dominated by
189 EBFs, located entirely in Mediterranean Europe (MED), and about 10% (92'209 km²) was
190 dominated by DBF which was largely distributed across MED. Approximately 20%
191 (174'934 km²) of the total forested area was dominated by MFs largely dominating Central
192 Europe (CEU), and about 47% (427'529 km²) was dominated by WSA mostly found in
193 NEU (Figure 1).

194



195
 196 **Figure 1** Spatial coverage of forests (ENF - evergreen needleleaf forest; EBF - evergreen
 197 broadleaf forest; DBF - deciduous broadleaf forest; MF - mixed forest), and woodlands
 198 (WSA - woody savannas) across Europe. Areas are differentiated into Northern Europe
 199 (NEU), Central Europe (CEU), and Mediterranean Europe (MED) following Markonis et
 200 al. (2021). The map is based on MODIS land cover product MCD12C1 (version 6.1).

201 *Drought detection and statistical data analysis*

202 The focus of our analysis was on the summer months during three extreme years of 2003,
 203 2018 and 2022. For this purpose, we subset VPD, soil moisture (SM), and both vegetation
 204 proxies (NIRv and GOSIF) for the months of June, July, August (JJA) which consisted of
 205 fourteen 8-day periods, for each forested pixel between 2000 and 2022. We restricted
 206 our analysis to the months of June-July-August so our study is 1) comparable with existing
 207 studies focused on the summer drought 2) to capture the peak of the warm and dry
 208 conditions across Europe, that would be most stressful for the vegetation functioning,
 209 from the perspective of heat and water supply.

210 To account for the impact of the observed greening trend across Europe on vegetation
211 proxy anomalies during the extreme years (2003, 2018, 2022), we applied a detrending
212 process to the summer mean NIRv and GOSIF data. This detrending was performed
213 pixel-wise from 2000 to 2022 using a simple linear regression model (Buras et al., 2020).
214 We then calculated pixel-wise standardized summer anomalies, expressed as z-scores
215 (Var_z), for all variables—VPD, SM, and the detrended NIRv and GOSIF (hereafter
216 referred to as NIRv and GOSIF)—for each year, including the extreme years, using
217 Equation 3.

218

$$219 \quad Var_z \text{ (unitless)} = \frac{Var - Var_{mean}}{Var_{sd}} \quad (3)$$

220

221 where, Var_{mean} and Var_{sd} are mean and standard deviation of any variable over the 2000-
222 2022 period.

223

224 In drought identification studies, classification of ‘normal’ (not to be confused with normal
225 distribution), ‘drought’ (used synonymously with ‘dry’), or ‘wet’, is largely done using a
226 standardized index, such as SPI (Standardized Precipitation Index), SPEI (Standardized
227 Precipitation Evapotranspiration Index), and z-score among others (see Mishra and
228 Singh, 2011). All studies that use a standardized index for classification, classify “normal”
229 conditions when the index is between -1 and 1, and “below normal” conditions when the
230 index is < -1 , and “above normal” conditions when the index > 1 (Jain et al., 2015, Wable
231 et al., 2019, Dogan et al., 2012, Tsakiris and Vangelis, 2005). In this study, we classified
232 drought conditions as occurring when soil moisture is below normal ($SM_z < -1$) and VPD
233 is above normal ($VPD_z > 1$), indicating both soil AND atmospheric dryness. This
234 threshold-based approach using standardized anomalies aligns with established methods
235 for drought identification and is pertinent for studying drought impacts on forests. Both
236 soil moisture and VPD directly affect vegetation functioning, making them effective
237 proxies for identifying environmental constraints on plant physiological performance.
238 Furthermore, such classification of ‘normal’ (and thus, ‘above normal’ and ‘below normal’
239 used in this study) based on z-scores (also called standardized anomalies) can be done

240 for any meteorological and/or response variables, such as NIRv and GOSIF done in this
241 study, making the narration of results coherent across different variables.

242 We used the Pearson correlation coefficient (r) and partial correlation coefficients (Pr) to
243 understand the spatial (across space for each year) and temporal (during each year)
244 correlation of GOSIF and NIRv anomalies with SM and VPD anomalies (Dang et al.,
245 2022). We calculated the partial correlation coefficient using equations 4-7:

246

$$247 \quad Pr(GOSIF, SM) = \frac{r(GOSIF, SM) - r(GOSIF, VPD) \times r(SM, VPD)}{\sqrt{1 - r(GOSIF, VPD)^2} - \sqrt{1 - r(SM, VPD)^2}} \quad (4)$$

248

$$249 \quad Pr(GOSIF, VPD) = \frac{r(GOSIF, VPD) - r(GOSIF, SM) \times r(SM, VPD)}{\sqrt{1 - r(GOSIF, SM)^2} - \sqrt{1 - r(SM, VPD)^2}} \quad (5)$$

250

$$251 \quad Pr(NIRv, SM) = \frac{r(NIRv, SM) - r(NIRv, VPD) \times r(SM, VPD)}{\sqrt{1 - r(NIRv, VPD)^2} - \sqrt{1 - r(SM, VPD)^2}} \quad (6)$$

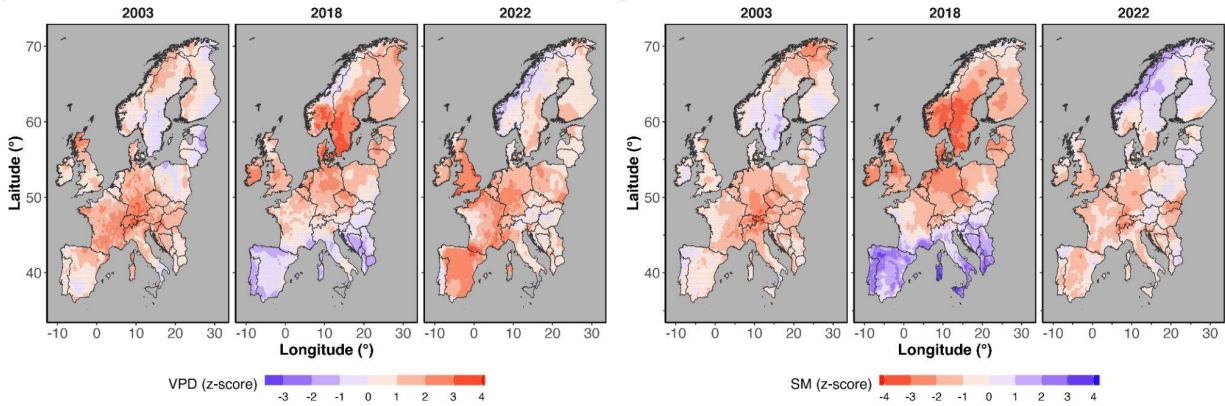
252

$$253 \quad Pr(NIRv, VPD) = \frac{r(NIRv, VPD) - r(NIRv, SM) \times r(SM, VPD)}{\sqrt{1 - r(NIRv, SM)^2} - \sqrt{1 - r(SM, VPD)^2}} \quad (7)$$

254 **Results**

255 *Severity of the 2022 summer drought compared to 2018 and 2003*

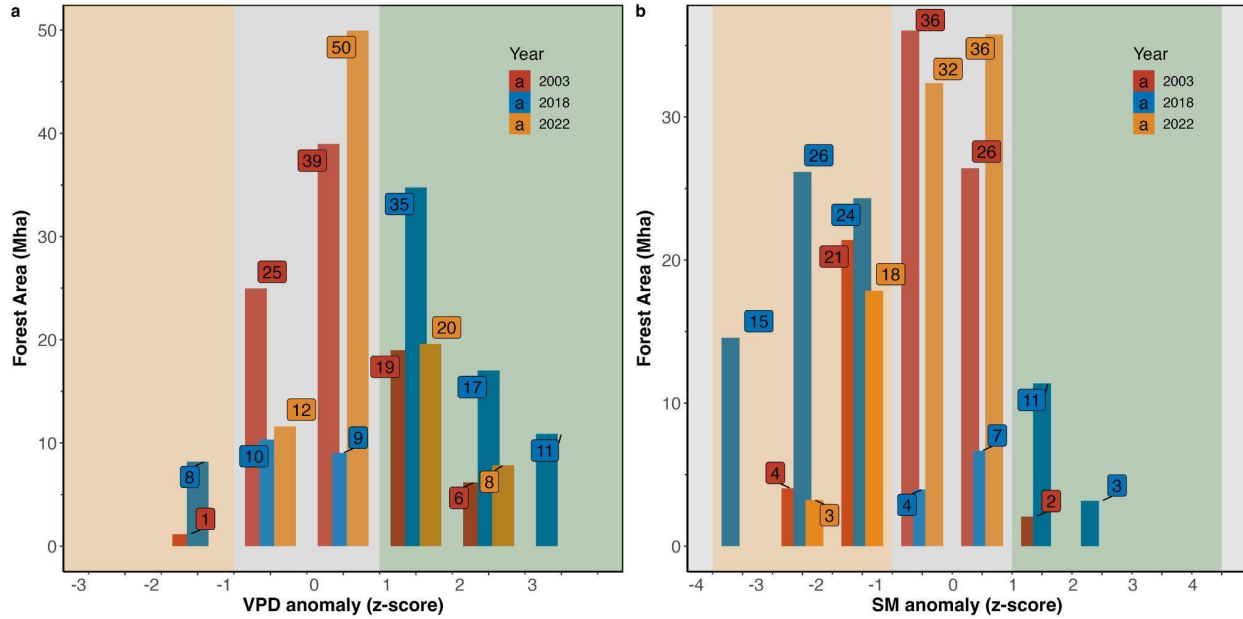
256 Figure 2 shows the extent and magnitude of anomalies (z-score) of VPD and top layer (0-
257 7 cm) soil moisture content during the summer months in 2003, 2018, and 2022 across
258 Europe. In summer 2022, particularly southern regions of Europe experienced the most
259 pronounced increase in atmospheric (z-score > 1) and soil dryness (z-score < -1) (Figure
260 2) while in 2018 we observed the most widespread VPD and SM anomalies in northern
261 Europe (Figure 2).



262
 263 **Figure 2** Standardized summer (JJA) anomalies (z-score) of mean vapor pressure deficit
 264 (VPD), and top layer (1-7 cm depth) soil moisture (SM) in 2003, 2018 and 2022, across
 265 the region of Europe.

266
 267 Figure 3 shows the intensity of atmospheric and soil drought via z-score values of VPD
 268 and SM anomalies over the summer months (JJA) in 2003, 2018, and 2022. The total
 269 affected area displayed in Figure 3 is the sum of all pixels within the given z-score bin
 270 during the summer period where z-scores are averaged for each bin for the summer
 271 period. Restricted to forested areas, atmospheric and soil drought was 55% and 58%
 272 more extensive in 2018 compared to 2022, and in both years more extensive than in 2003
 273 (Figure 3). In 2022, 28 Mha of forested areas in Europe experienced an extremely high
 274 VPD (z-score > 1), while in 2018, 63 Mha experienced such extreme conditions. In 2022,
 275 21 Mha of forested areas experienced an extremely low soil moisture content (z-score <
 276 -1) while in 2018, 50 Mha of forests in Europe were affected by such extreme conditions.
 277 In 2003 an area of 25 Mha was affected by extremely dry air and a similar area was
 278 affected by extremely dry soil (Figure 3). A comparison of soil drought detected from SM
 279 at 0-100 cm showed a similar result in terms of drought severity and spatial coverage and
 280 thus we used SM at 0-7 cm soil layer for our analysis (see Supplementary Figure 1).

281

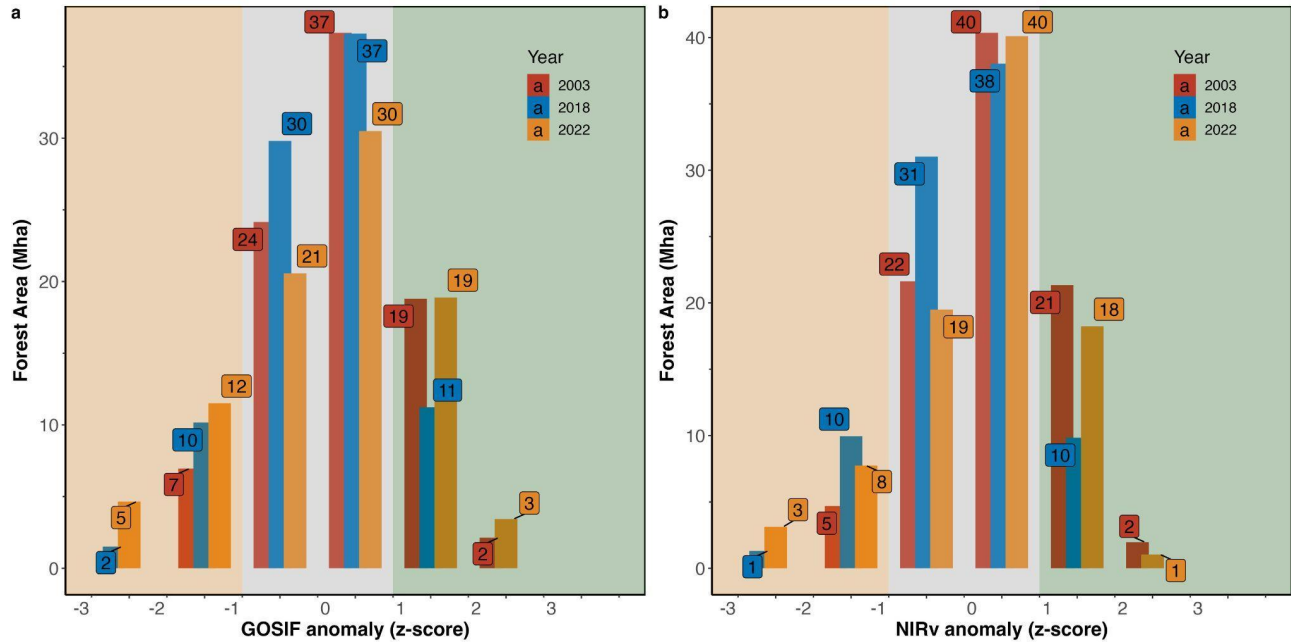


282
 283 **Figure 3** Intensity (z-score) and extent (area affected, Mha) of (a) VPD, and (b) SM
 284 anomalies across forested areas during the summer months (JJA). Z-score, values from
 285 -1 and 1 are considered normal (within 1 standard deviation of the mean). Orange-shaded
 286 area marks below normal and green-shaded area marks above normal conditions.

287
 288 *Forest canopy response to the 2022 drought*

289 The intensity of GOSIF and NIRv anomalies over the summer months (JJA) in 2003,
 290 2018, and 2022 are displayed in Figure 4. The extent shown in Figure 4 is the sum of all
 291 pixels within the given z-score bin during the summer period (z-scores are averaged for
 292 each bin). Compared to 2018, the extremely dry conditions in 2022 led to 30% increase
 293 in forested areas that exhibited declined photosynthesis (17 Mha in 2022 compared to 12
 294 Mha in 2018) (Figure 4). The extent of the canopy browning observed in 2022 was similar
 295 to 2018, which in both years was 120% of the extent of observed canopy browning in
 296 2003 (11 Mha compared to 5 Mha observed in 2003) (Figure 4).

297



298
299

300 **Figure 4** Intensity (z-score) and extent (area affected, Mha) for (a) GOSIF, and (b) NIRv
301 anomalies across forested areas during the summer months (JJA). Z-score, values from
302 -1 and 1 are considered normal (within 1 standard deviation of the mean). Orange-shaded
303 area marks below normal and green-shaded area marks above normal conditions.

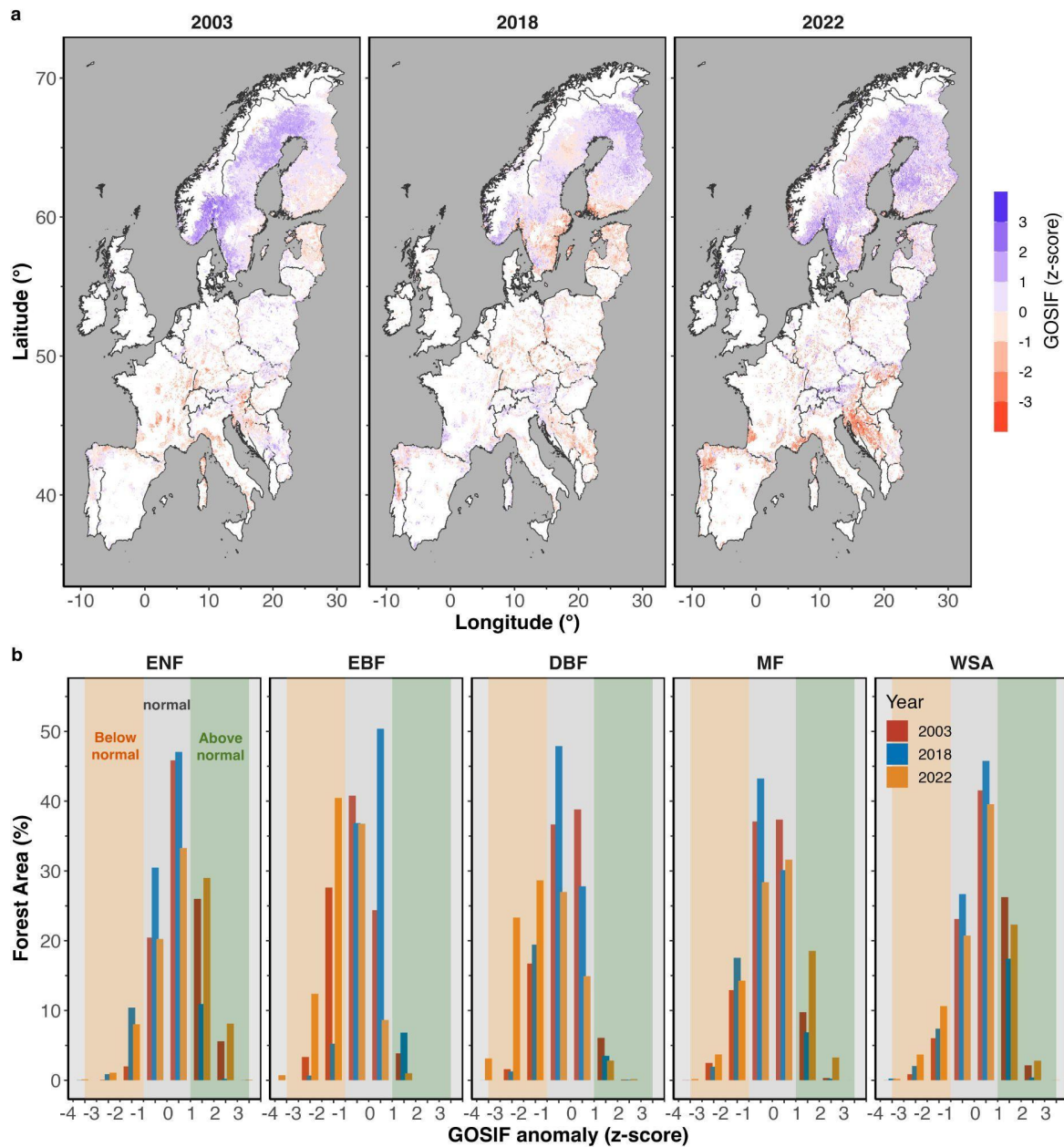
304

305 Figure 5a shows the GOSIF anomalies (z-score) across all forested areas in Europe. The
306 intensity and extent of the GOSIF anomalies during the summer months (JJA) in each
307 year are shown for different forest types in Figure 5b. Across specific forest types, DBFs
308 showed the largest negative GOSIF anomaly in 2022 but the ENFs showed a positive
309 GOSIF anomaly in 2022, both in terms of magnitude and in terms of the spatial extent of
310 negative GOSIF anomalies (Figure 5).

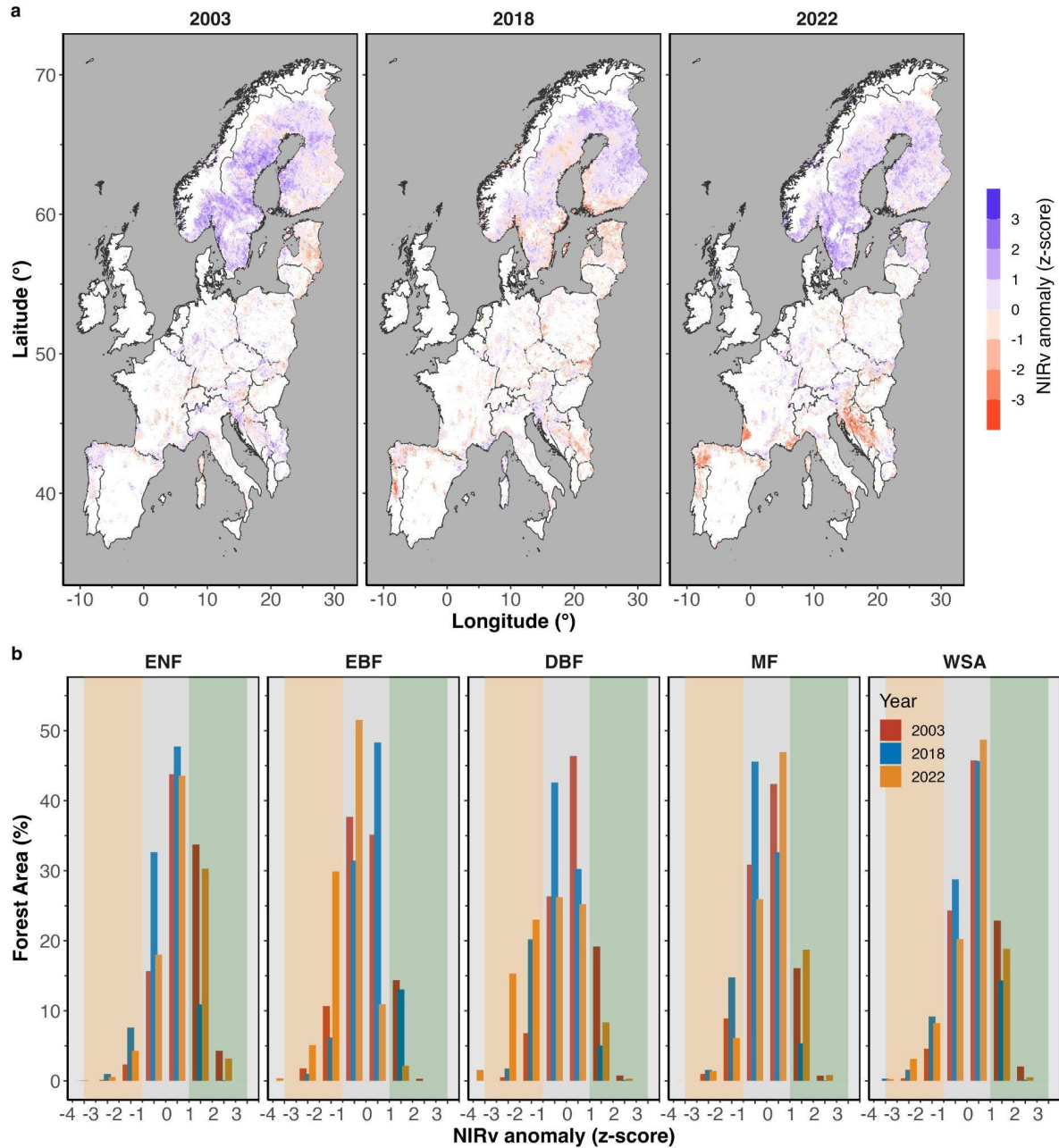
311

312 Figure 6a shows the anomalies of NIRv (average z-score over the summer months)
313 across all forested areas in Europe. The intensity and extent of the NIRv anomalies during
314 the summer months (JJA) in each year are shown for different forest types in Figure 6b.
315 In terms of canopy browning response (NIRv anomalies), the largest negative NIRv
316 anomalies (indicated by the maximum anomaly) were observed in the DBFs in 2022,

317 fitting the declined GOSIF signals. The ENFs showed positive NIRv anomalies in 2022,
 318 in terms of magnitude, spatial coverage, and % of total area affected (Figure 6).



319
 320 **Figure 5** (a) GOSIF anomaly (in terms of z-score) across Europe, and (b) area coverage
 321 (in terms of percentage of total area for each forest type) during the summer months (JJA)
 322 in 2003, 2018 and 2022. Orange-shaded area marks below normal and green-shaded
 323 area marks above normal conditions. White areas on the map mark non-forested regions.
 324



325

326 **Figure 6** (a) NIRv anomaly (in terms of z-score) across Europe, and (b) area coverage

327 (in terms of percentage of total area for each forest type) during the summer months (JJA)

328 in 2003, 2018 and 2022. In panel (b) Orange-shaded area marks below normal and green-

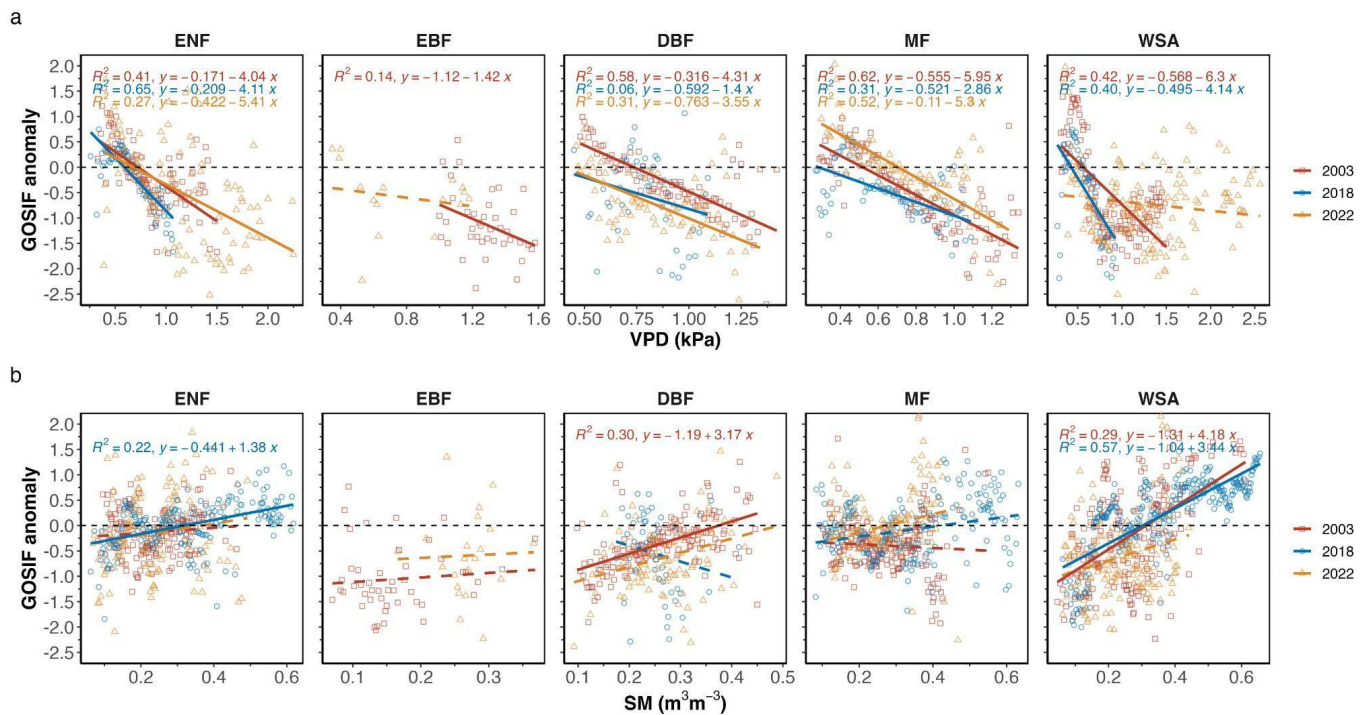
329 shaded area marks above normal conditions. White areas on the map mark non-forested

330 regions.

331

332 *Relationship between GOSIF and NIRv*

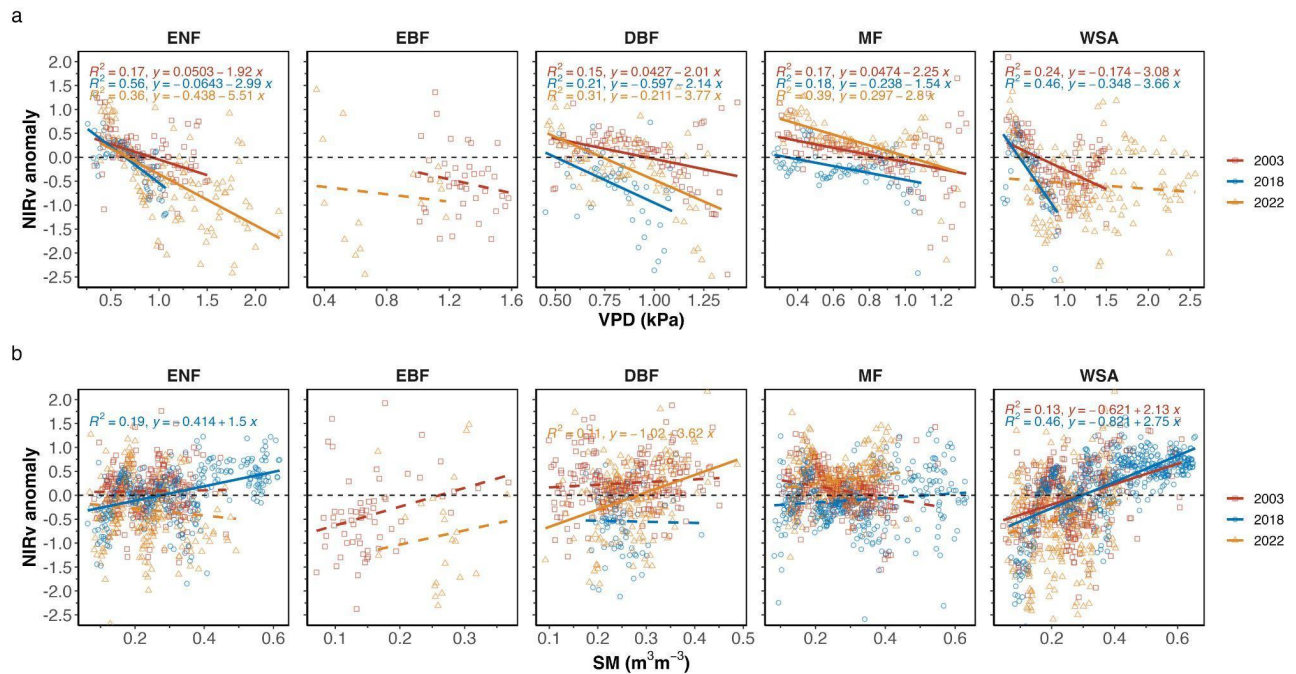
333 In general, the values of NIRv and GOSIF were highly correlated (Supplementary Figure
 334 2). The anomalies of NIRv and GOSIF were most correlated across WSAs ($r^2 = 0.73$ in
 335 2018) and least correlated across the ENFs (Supplementary Figure 2). Figure 7 shows
 336 the spatial regression between standardized GOSIF anomalies with (a) VPD and (b) SM
 337 and Figure 8 shows the spatial regression between standardized NIRv anomalies with (a)
 338 VPD and (b) SM over the drought areas in summers 2003, 2018 and 2022. With the
 339 increase in VPD (i.e., increased atmospheric dryness), GOSIF values declined across all
 340 forest types, across all years, except in 2022 in the WSA, and in 2018 and 2022 in EBFs
 341 (Figure 7). With decrease in soil moisture (i.e., increased soil dryness), GOSIF values
 342 also declined overall ($r^2 = 0.34$), but not as strongly as with the increase in air dryness (r^2
 343 $= 0.39$) (Figure 7). Across different forest types, GOSIF responded most strongly to VPD
 344 anomalies in the MFs (mean $r^2 = 0.48$), and responded most directly to changes in the
 345 soil moisture in the WSA (Figure 7).



346
 347 **Figure 7** Spatial regression between standardized GOSIF anomalies with (a) VPD and
 348 (b) SM over the drought areas during the summer months (JJA) 2003, 2018 and 2022.
 349 Dashed lines mark an insignificant relationship ($p > 0.05$).

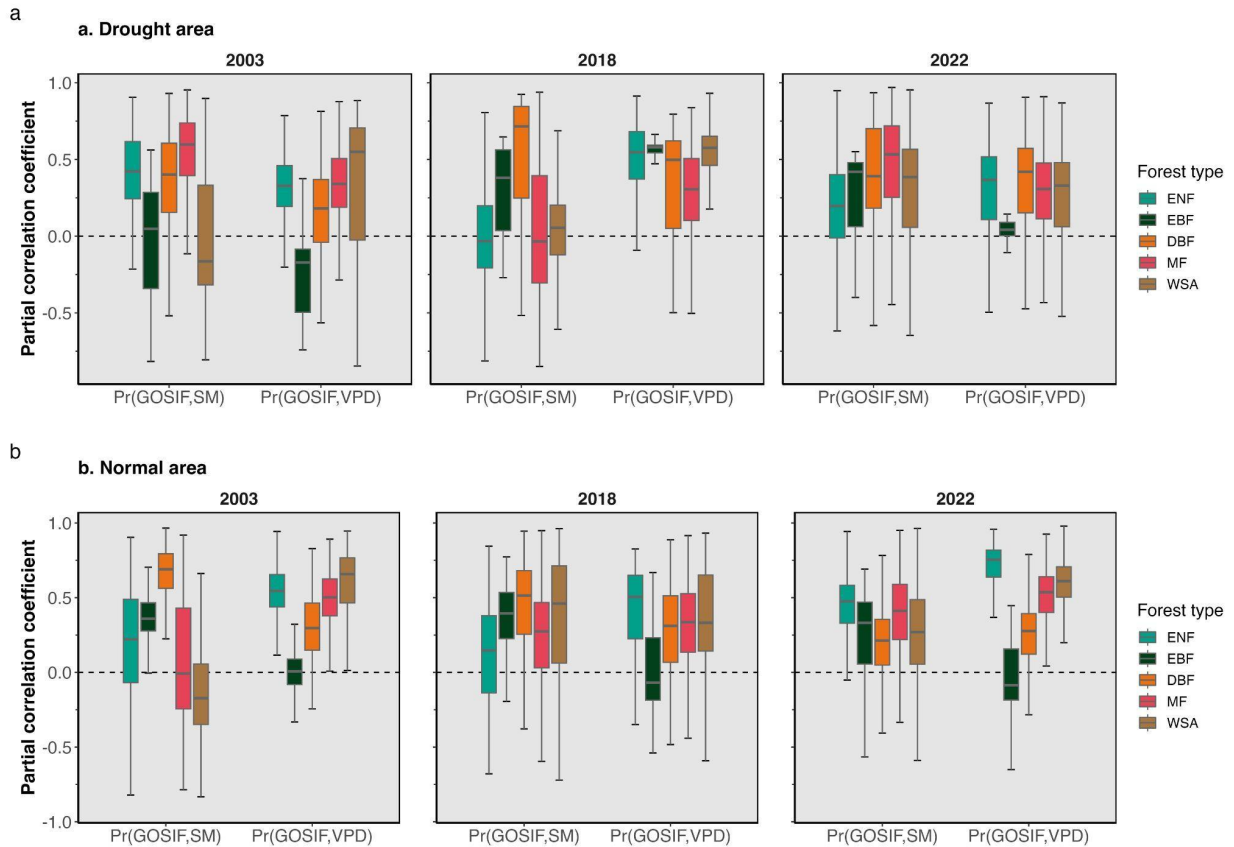
350

351 Between VPD and SM, in general GOSIF anomalies were more correlated with VPD than
 352 with SM anomalies, and the decline in VPD correlated well with the larger GOSIF decline
 353 that we observed in DBFs in 2022 and in ENFs in 2003 (Figure 7). Under typical
 354 conditions (regardless of drought), GOSIF's response to both air dryness and soil
 355 moisture anomalies was more pronounced than the response of NIRv ($r^2 = 0.39$ with
 356 GOSIF, compared to $r^2 = 0.29$ for NIRv) (Figure 7, 8).
 357 Figure 9 shows the partial correlation coefficient between GOSIF with SM and VPD during
 358 summer months (JJA) for areas identified as affected (Figure 9a) and not affected (Figure
 359 9b) by drought. The SM and VPD values across all forest types correlated well, but across
 360 DBFs the dryness in the atmosphere and the dryness in the soil were most correlated
 361 (Figure 9). Regarding canopy response to VPD, European Needleleaf Forests (ENF)
 362 exhibited the strongest reaction to changes in atmospheric dryness (Figure 9)



363
 364 **Figure 8.** Spatial (over all pixels) regression between standardized NIRv anomalies with
 365 (a) VPD and (b) SM over the drought areas and normal areas in 2003, 2018 and 2022
 366 during the summer months (JJA).

367
 368



369
 370 **Figure 9.** Temporal partial correlation coefficient of GOSIF with the absolute values of
 371 SM and VPD during the summer months (JJA) in 2003, 2018 and 2022, for detected (a)
 372 drought areas and (b) normal areas. A comparable figure for NIRv can be found in
 373 Supplementary Figure 3.

374 Discussion

375 *Severity of the 2022 summer drought*

376 Although the years 2003, 2018, and 2022 are all categorized as "extreme," the specific
 377 characteristics of the extreme conditions varied significantly among these years. For
 378 example, in 2003, widespread negative anomalies in soil moisture signaled a significant
 379 soil drought, whereas in 2022, widespread positive VPD anomalies indicated a notably
 380 drier atmosphere (Figure 3). It is important to note that ERA-5 Land datasets have been
 381 shown to underestimate the extent of European heatwaves in 2003, 2010, and 2018
 382 (Duveiller et al., 2023), partly due to the use of a static leaf area index in their modeling

383 framework. Consequently, the SM droughts in the years 2003, 2018, and 2022 may be
384 more severe than indicated by our study, suggesting that our results might be somewhat
385 conservative. The extensive summer drought in 2022 primarily impacted southern
386 Europe, in contrast to the 2003 summer drought, which affected central Europe, and the
387 2018 drought, which extended to central and northern Europe (Figure 2) (Bastos et al.,
388 2020). Consequently, the severe dry conditions in 2022 resulted in an average decline in
389 GOSIF across forests that was 30% more widespread compared to 2018, and 60% more
390 widespread compared to 2003 (Figure 4). These above-normal dry conditions during the
391 summer reduced the photosynthetic capacity of plants and, consequently, the
392 ecosystem's ability to absorb carbon from the atmosphere (Peters et al., 2018; van der
393 Woude et al., 2023). Although the atmospheric and soil droughts in 2018 were more
394 extensive and severe compared to 2022 (as indicated by the maximum observed z-
395 scores), the adverse impact on forests, as reflected by the decline in GOSIF, was greater
396 in 2022.

397 *Canopy response to soil versus atmospheric dryness*

398 The GOSIF dataset used in this study has been shown to be a reliable proxy for
399 vegetation gross productivity, as demonstrated by comparisons with ground-based flux
400 measurements (Shekhar et al. 2022; Pickering et al. 2022). It is important to note that
401 GOSIF estimates are derived from a machine learning model trained with OCO-2 SIF
402 observations, MODIS EVI data, and meteorological reanalysis data. As a result, the
403 meteorological data used in our analyses are not entirely independent of the SIF data.
404 However, this overlap is unlikely to impact our findings. A recent study that compared
405 GOSIF with original OCO-2 data to assess the impacts of the 2018 U.S. drought found
406 similar responses to drought between the two datasets (Li et al., 2020).

407 NIRv and SIF signals are well-correlated and effectively capture seasonal patterns in GPP
408 (Getachew Mengistu et al. 2021). Although the strength of their relationship can vary with
409 time, location, and forest type (see Supplementary Figure 2), reductions in SIF signals
410 are directly associated with decreased photosynthesis. While both SIF and NIRv are
411 reliable indicators of canopy responses to extreme climate events, SIF is more responsive
412 to short-term climatic changes (Figure 7).

413 Our analysis showed that across different regions, GOSIF anomalies corresponded more
414 strongly to increased atmospheric dryness than to increased soil dryness (Figure 7). This
415 supports the understanding that vapor pressure deficit plays a larger role in controlling
416 SIF signals for trees over shorter time scales than soil moisture (Pickering et al. 2022).
417 Over shorter time frames, trees can often mitigate soil moisture deficits through
418 mechanisms within the rooting zone and by accessing deeper water sources, whereas
419 there is no such buffer for the impact of atmospheric dryness on tree canopies.

420 Ground-based observations in forest ecosystems, including both ecosystem and tree-
421 level measurements, have shown that atmospheric dryness can constraint canopy gas
422 exchange, even when soil moisture is not limiting (Gharun et al. 2014, Fu et al. 2022,
423 Shekhar et al. 2024a). These findings highlight the importance of considering atmospheric
424 dryness as a limiting factor for tree photosynthesis during extremely dry conditions and
425 demonstrate the rapid response of various canopy types to increased levels of
426 environmental dryness.

427 *Canopy response to drought across different forest types*

428 The spread of drought, measured as the total area across z-scores, exhibited distinct
429 patterns in different years, leading to varied responses of different forest types to the
430 climatic anomalies. Impact of drought on forests can significantly differ depending on the
431 forest type, tree species, species composition, and past exposure to extreme conditions
432 (Arthur and Dech 2016; Chen et al. 2022). Our analysis showed that conditions in summer
433 2022 reduced vegetation functioning across DBFs the most, as it was indicated by
434 declined GOSIF signals (Figure 5). While deciduous broad-leaved forests were most
435 negatively affected by the extreme conditions in 2022, Evergreen Needle-Leaf Forests
436 (ENF) distributed in northern regions of Europe were not exposed to extremely dry
437 conditions in 2022 and even showed enhanced canopy greening and GOSIF signals,
438 through benefiting from the episodic warming (Forzieri et al. 2022). Under similar drought
439 conditions, the mechanisms to cope with the level of drought stress vary largely among
440 forest types, and depend on a combination of characteristics that control water loss
441 through the coordination of stomatal regulation, hydraulic architecture, and root
442 characteristics (e.g., rooting depth, root distribution, root morphology) (Gharun et al. 2020;

443 Peters et al. 2023). Stomata of trees exhibit a high sensitivity to VPD fluctuations, causing
444 a reduction in stomatal conductance as VPD increases, which, in turn, limits the exchange
445 of CO₂ with the atmosphere during photosynthesis (Bonal and Guehl in 2011; Li et al.
446 2023). Different tree species show varying degrees of sensitivity in their stomatal
447 responses to atmospheric dryness (Oren et al., 1999). For example, ring-porous species
448 tend to maintain robust gas exchange under dry conditions, while diffuse-porous species,
449 like those in ENFs, exhibit stronger stomatal regulation, reducing stomatal conductance
450 as water availability decreases (Klein, 2014). This variability places plants on a spectrum
451 of drought tolerance, reflecting their specific water relations strategies and leading to
452 different responses among forests in similar climatic regions.

453 *Vulnerability of forests to more frequent drought*

454 The increased canopy damage observed in 2022, despite less severe conditions
455 compared to the previous extreme year, suggests a lasting impact on forest canopies that
456 could lead to a decline in forest resilience in the face of more frequent drought events
457 (Forzieri et al., 2022). A potential decline in the resilience of forests has significant
458 implications for vital ecosystem services, including the forest's capacity to mitigate climate
459 change. Consequently, there is an urgent need to consider these trends when formulating
460 robust forest-based mitigation strategies. This need is especially critical given future
461 projections indicating that the frequency and intensity of extreme dryness across Europe
462 will more than triple by the end of the 21st century (Shekhar et al., 2024b). In this context,
463 it is increasingly important to investigate the vulnerability of forests to external
464 perturbations and to develop mitigation strategies tailored to site-specific
465 ecophysiological and environmental factors that influence forest resilience to drought.
466 Effective management strategies should be based on an understanding of these factors
467 to mitigate the legacy effects of drought (McDowell et al., 2020; Wang et al., 2023;
468 Shekhar et al., 2024a).

469

470 **Conclusion**

471 The severity of the 2022 summer drought, marked by increased atmospheric dryness,
472 significantly compromised the photosynthetic capacity of trees, leading to widespread
473 declines in vegetation functioning, especially in deciduous broad-leaved forests. Our

474 findings underscore the importance of considering atmospheric dryness as a critical factor
475 influencing canopy responses during extreme climatic events, alongside soil moisture
476 deficits. Despite less severe overall conditions compared to previous extreme years, the
477 greater canopy damage observed in 2022 suggests a growing vulnerability of forests to
478 drought. This raises concerns about the future climate mitigation capacity of forest
479 ecosystems, particularly as projections indicate a continued increase in the frequency and
480 intensity of extreme dryness across Europe.

481

482 **Competing interests**

483 The authors have no competing interests to declare.

484

485 **Acknowledgements**

486 AS acknowledges funding from the SNF funded project EcoDrive (IZCOZO_198094).

487

488 **References**

- 489 Albergel, C., De Rosnay, P., Balsamo, G., Isaksen, L., Munoz-Sabater, J., 2012. Soil
490 moisture analyses at ECMWF: evaluation using global ground-based in situ
491 observations. *J. Hydrometeorol.* 13, 1442–1460. <https://doi.org/10.1175/JHM-D11-0107.1>.
- 492 Anjileli, H., Huning, L.S., Mofstakhari, H. et al. (2021) Extreme heat events heighten soil
493 respiration. *Sci Rep* 11, 6632. <https://doi.org/10.1038/s41598-021-85764-8>
- 494 Arthur CM, Dech JP (2016) Species composition determines resistance to drought in dry forests
495 of the Great Lakes - St. Lawrence forest region of central Ontario. *Journal of Vegetation Science*
496 27, 914-925.
- 497 Badgley G et al. (2017) Canopy near-infrared reflectance and terrestrial photosynthesis. *Sci.*
498 *Adv.* 3, e1602244. DOI:10.1126/sciadv.1602244
- 499 Bastos A et al. (2020) Impacts of extreme summers on European ecosystems: a comparative
500 analysis of 2003, 2010 and 2018. *Phil. Trans. R. Soc. B* 375: 20190507.
501 <http://dx.doi.org/10.1098/rstb.2019.0507>
- 502 Bauke, S. L., Amelung, W., Bol, R., Brandt, L., Brüggemann, N., Kandeler, E., Meyer, N., Or,
503 D., Schnepf, A., Schloter, M., Schulz, S., Siebers, N., von Sperber, C., & Vereecken, H. (2022).
504 Soil water status shapes nutrient cycling in agroecosystems from micrometer to landscape
505 scales. *Journal of Plant Nutrition and Soil Science*, 185, 773–792.
506 <https://doi.org/10.1002/jpln.202200357>
- 507 Bonal, D. & Guehl, J.-M. (2011) Contrasting patterns of leaf water potential and gas exchange
508 responses to drought in seedlings of tropical rainforest species. *Functional Ecology*, 15, 490–
509 496.
- 510 Buras, A., Rammig, A., and Zang, C. S. (2020) Quantifying impacts of the 2018 drought on
511 European ecosystems in comparison to 2003, *Biogeosciences*, 17, 1655–1672,
512 <https://doi.org/10.5194/bg-17-1655-2020>.
- 513 Chen, Y., Vogel, A., Wagg, C. et al. (2022) Drought-exposure history increases complementarity
514 between plant species in response to a subsequent drought. *Nat Commun* 13, 3217.
515 <https://doi.org/10.1038/s41467-022-30954-9>
- 516 Choat, B., Brodribb, T.J., Brodersen, C.R. et al. (2018) Triggers of tree mortality under drought.
517 *Nature* 558, 531–539. <https://doi.org/10.1038/s41586-018-0240-x>
- 518 Cornes, R. C., van der Schrier, G., van den Besselaar, E. J. M., & Jones, P. D. (2018). An
519 Ensemble Version of the E-OBS Temperature and Precipitation Data Sets. *Journal of*
520 *Geophysical Research: Atmospheres*, 123(17), 9391–9409.
521 <https://doi.org/10.1029/2017JD028200>

522 Dang, C., Shao, Z., Huang, X., Qian, J., Cheng, G., Ding, Q., & Fan, Y. (2022). Assessment of
523 the importance of increasing temperature and decreasing soil moisture on global ecosystem
524 productivity using solar-induced chlorophyll fluorescence. *Global Change Biology*, 28(6), 2066–
525 2080. <https://doi.org/10.1111/gcb.16043>
526

527 Dee, D. P., Uppala, S. M., Simmons, A. J., Berrisford, P., Poli, P., Kobayashi, S., Andrae, U.,
528 Balmaseda, M. A., Balsamo, G., Bauer, P., Bechtold, P., Beljaars, A. C. M., van de Berg, L.,
529 Bidlot, J., Bormann, N., Delsol, C., Dragani, R., Fuentes, M., Geer, A. J., Haimberger, L., Healy,
530 S. B., Hersbach, H., Hólm, E. V., Isaksen, L., Kållberg, P., Köhler, M., Matricardi, M., McNally,
531 A. P., Monge-Sanz, B. M., Morcrette, J. J., Park, B. K., Peubey, C., de Rosnay, P., Tavolato,
532 C., Thépaut, J. N., and Vitart, F. (2011) The ERA-Interim reanalysis: configuration and
533 performance of the data assimilation system, *Quarterly Journal of the Royal Meteorological*
534 *Society*, 137, 121 553-597, [10.1002/qj.828](https://doi.org/10.1002/qj.828).

535 S. Dogan, A. Berktaç, V.P. Singh (2012) Comparison of multi-monthly rainfall-based drought
536 severity indices, with application to semi-arid Konya closed basin, Turkey
537 *J. Hydrol.*, 470–471, pp. 255-268
538

539 Drake JE, Tjoelker MG, Vårhammar A, Medlyn BE, Reich PB, Leigh A, Pfautsch S, Blackman
540 CJ, López R, Aspinwall MJ, Crous KY, Duursma RA, Kumarathunge D, De Kauwe MG,
541 Jiang M, Nicotra AB, Tissue DT, Choat B, Atkin OK, Barton CVM (2018) Trees tolerate an
542 extreme heatwave via sustained transpirational cooling and increased leaf thermal tolerance.
543 *Glob Change Biol.* 24: 2390–2402. <https://doi.org/10.1111/gcb.14037>
544

545 Duveiller, G., Pickering, M., Muñoz-Sabater, J., Caporaso, L., Boussetta, S., Balsamo, G., and
546 Cescatti, A. (2023) Getting the leaves right matters for estimating temperature extremes,
547 *Geosci. Model Dev.*, 16, 7357–7373, <https://doi.org/10.5194/gmd-16-7357-2023>.
548

549 Forzieri, G., Dakos, V., McDowell, N.G. et al. (2022) Emerging signals of declining forest
550 resilience under climate change. *Nature* 608, 534–539. [https://doi.org/10.1038/s41586-022-](https://doi.org/10.1038/s41586-022-04959-9)
551 [04959-9](https://doi.org/10.1038/s41586-022-04959-9)

552 Fu, Z., Ciais, P., Prentice, I.C. et al. Atmospheric dryness reduces photosynthesis along a large
553 range of soil water deficits. *Nat Commun* 13, 989 (2022). [https://doi.org/10.1038/s41467-022-](https://doi.org/10.1038/s41467-022-28652-7)
554 [28652-7](https://doi.org/10.1038/s41467-022-28652-7)
555

556 Gessler, A., Bottero, A., Marshall, J. and Arend, M. (2020), The way back: recovery of trees
557 from drought and its implication for acclimation. *New Phytol*, 228: 1704-1709.
558 <https://doi.org/10.1111/nph.16703>

559 Getachew Mengistu, A., Mengistu Tsidu, G., Koren, G., Kooreman, M. L., Folkert Boersma, K.,
560 Tagesson, T., Ardö, J., Nouvellon, Y., & Peters, W. (2021). Sun-induced fluorescence and near-
561 infrared reflectance of vegetation track the seasonal dynamics of gross primary production over
562 Africa. *Biogeosciences*, 18(9), 2843-2857. <https://doi.org/10.5194/bg-18-2843-2021>

- 563 Gharun M., Vervoort R.W., Turnbull T.L., Adams M.A. (2014) A test of how coupling of
564 vegetation to the atmosphere and climate spatial variation affects water yield modelling in
565 mountainous catchments 514, pp. 202-213. <https://doi.org/10.1016/j.jhydrol.2014.04.037>
- 566 Gharun M., Hörtnagl L., Paul-Limoges E., Ghiasi S., Feigenwinter I., Burri S., Marquardt K.,
567 Etzold S., Zweifel R., Eugster W., Buchmann N (2020) Physiological response of Swiss
568 ecosystems to 2018 drought across plant types and elevation *Phil. Trans. R. Soc.*
569 *B3752019052120190521*. <http://doi.org/10.1098/rstb.2019.0521>
- 570 Gourlez de la Motte L, Beauclaire Q, Heinesch B, Cuntz M, Foltýnová L, Šigut L, Kowalska N,
571 Manca G, Ballarin IG, Vincke C, Roland M, Ibrom A, Lousteau D, Siebicke L, Neiryink J,
572 Longdoz B. (2020) Non-stomatal processes reduce gross primary productivity in temperate
573 forest ecosystems during severe edaphic drought. *Philos Trans R Soc Lond B Biol Sci.*
574 *375(1810):20190527*. doi: 10.1098/rstb.2019.0527.
- 575 Haesen, S., Lembrechts, J. J., De Frenne, P., Lenoir, J., Aalto, J., Ashcroft, M. B., Kopecký, M.,
576 Luoto, M., Maclean, I., Nijs, I., Niittynen, P., van den Hoogen, J., Arriga, N., Brúna, J.,
577 Buchmann, N., Čiliak, M., Collalti, A., De Lombaerde, E., Descombes, P. ... Van Meerbeek, K.
578 (2023). ForestClim—Bioclimatic variables for microclimate temperatures of European forests.
579 *Global Change Biology*, 29, 2886–2892. <https://doi.org/10.1111/gcb.16678>
- 580 Humphrey V, Zscheischler J, Ciais P, Gudmundsson L, Sitch S, Seneviratne SI. (2018)
581 Sensitivity of atmospheric CO₂ growth rate to observed changes in terrestrial water storage.
582 *Nature*, 560 (7720): 628 DOI: 10.1038/s41586-018-0424-4.
- 583 Jain VK, Pandey RP, Jain MK, Byun HR (2015) Comparison of drought indices for appraisal of
584 drought characteristics in the Ken River Basin, *Weather and Climate Extremes* 8, 1-11,
585 <https://doi.org/10.1016/j.wace.2015.05.002>.
- 586 Klein Tank, A. M. G., Wijngaard, J. B., Können, G. P., Böhm, R., Demarée, G., Gocheva, A.,
587 Mileta, M., Pashiardis, S., Hejkrlik, L., Kern-Hansen, C., Heino, R., Bessemoulin, P., Müller-
588 Westermeier, G., Tzanakou, M., Szalai, S., Pálsdóttir, T., Fitzgerald, D., Rubin, S., Capaldo, M.,
589 ... Petrovic, P. (2002). Daily dataset of 20th-century surface air temperature and precipitation
590 series for the European Climate Assessment. *International Journal of Climatology*, 22(12),
591 1441–1453. <https://doi.org/10.1002/joc.773>
- 592 Klein, T. (2014), The variability of stomatal sensitivity to leaf water potential across tree species
593 indicates a continuum between isohydric and anisohydric behaviours. *Funct Ecol*, 28: 1313-
594 1320. <https://doi.org/10.1111/1365-2435.12289>
- 595 Lal, P., Shekhar, A., Gharun, M., Das, N.N., 2023. Spatiotemporal evolution of global
596 long-term patterns of soil moisture. *Sci. Total Environ.* 867, 161470 <https://doi.org/10.1016/j.scitotenv.2023.161470>.
- 597
598
599 Lal, P., Singh, G., Das, N.N., Colliander, A., Entekhabi, D., 2022. Assessment of ERA5-
600 land volumetric soil water layer product using in situ and SMAP soil moisture

601 observations. *Geosci. Rem. Sens. Lett. IEEE* 19, 1–5. <https://doi.org/10.1109/>
602 [LGRS.2022.3223985](https://doi.org/10.1109/LGRS.2022.3223985).

603 Li X et al. (2018) Solar-induced chlorophyll fluorescence is strongly correlated with terrestrial
604 photosynthesis for a wide variety of biomes: first global analysis based on OCO-2 and flux tower
605 observations *Glob. Change Biol.* 24 3990–4008.

606

607 Li, X., Xiao, J. (2019) A global, 0.05-degree product of solar-induced chlorophyll fluorescence
608 derived from OCO-2, MODIS, and reanalysis data. *Remote Sensing*, 11, 517;
609 [doi:10.3390/rs11050517](https://doi.org/10.3390/rs11050517).

610 Li X, Xiao J, Kimball JS, Reichle RH, Frankenberg C (2020) Synergistic use of SMAP and OCO-
611 2 data in assessing the responses of ecosystem productivity to the 2018 U.S. drought
612 *Remote Sens. Environ.* 251, 112062

613

614 Li, F., Xiao, J., Chen, J., Ballantyne, A., Jin, K., Li, B., Abraha, M., John, R. (2023) Global water
615 use efficiency saturation due to increased vapor pressure deficit. *Science*, 381, 672-677. DOI:
616 [10.1126/science.adf5041](https://doi.org/10.1126/science.adf5041).

617

618 Magney T S et al. (2019) Mechanistic evidence for tracking the seasonality of photosynthesis
619 with solar-induced fluorescence *Proc. Natl Acad. Sci. USA* 116 11640–5.

620

621 Marchin, R. M., Backes, D., Ossola, A., Leishman, M. R., Tjoelker, M. G., & Ellsworth, D. S.
622 (2022). Extreme heat increases stomatal conductance and drought-induced mortality risk in
623 vulnerable plant species. *Global Change Biology*, 28, 1133–1146.
624 <https://doi.org/10.1111/gcb.15976>

625

626 Markonis, Y., Kumar, R., Hanel, M., Rakovec, O., Máca, P., AghaKouchak, A., (2021). The rise
627 of compound warm-season droughts in Europe. *Science Advances* 7.
628 <https://doi.org/10.1126/sciadv.abb9668>

629

630 McDowell, N. G. et al. (2020) Pervasive shifts in forest dynamics in a changing world. *Science*
631 368, eaaz9463.

632

633 Mishra AK, Singh VP (2011) Drought modeling – A review, *Journal of Hydrology* 403(1–2),
634 157-175, <https://doi.org/10.1016/j.jhydrol.2011.03.049>.

635

636 Müller, L. M., and M. Bahn (2022) Drought legacies and ecosystem responses to subsequent
637 drought. *Global Change Biology* 28:5086–103. [doi:10.1111/gcb.16270](https://doi.org/10.1111/gcb.16270).

638

639 Muñoz-Sabater, J., Dutra, E., Agustí-Panareda, A., Albergel, C., Arduini, G., Balsamo, G.,
640 Boussetta, S., Choulga, M., Harrigan, S., Hersbach, H., Martens, B., Miralles, D. G., Piles, M.,
641 Rodríguez-Fernández, N. J., Zsoter, E., Buontempo, C., & Thépaut, J. N. (2021). ERA5-Land:
642 A state-of-the-art global reanalysis dataset for land applications. *Earth System Science Data*,
643 13(9), 4349–4383. <https://doi.org/10.5194/essd-13-4349-2021>

- 644 Peters, W., van der Velde, I.R., van Schaik, E. et al. Increased water-use efficiency and reduced
645 CO₂ uptake by plants during droughts at a continental scale. *Nature Geosci* 11, 744–748
646 (2018). <https://doi.org/10.1038/s41561-018-0212-7>
- 647 Peters, R.L., Steppe, K., Pappas, C., Zweifel, R., Babst, F., Dietrich, L., von Arx, G.,
648 Poyatos, R., Fonti, M., Fonti, P., Grossiord, C., Gharun, M., Buchmann, N., Steger, D.N.
649 and Kahmen, A. (2023), Daytime stomatal regulation in mature temperate trees
650 prioritizes stem rehydration at night. *New Phytol*, 239: 533-546.
651 <https://doi.org/10.1111/nph.18964>
- 652 Pickering, M., Cescatti, A., and Duveiller, G. (2022) Sun-induced fluorescence as a
653 proxy for primary productivity across vegetation types and climates, *Biogeosciences*,
654 19, 4833–4864, <https://doi.org/10.5194/bg-19-4833-2022>.
- 655 Oren, R., Sperry, J.S., Katul, G.G., Pataki, D.E., Ewers, B.E., Phillips, N. and Schäfer,
656 K.V.R. (1999), Survey and synthesis of intra- and interspecific variation in stomatal
657 sensitivity to vapour pressure deficit. *Plant, Cell & Environment*, 22: 1515-1526.
658 <https://doi.org/10.1046/j.1365-3040.1999.00513.x>
- 659 Rötthlisberger, M., Papritz, L. (2023). Quantifying the physical processes leading to
660 atmospheric hot extremes at a global scale. *Nature Geosci.* 16(3), 210-216.
661 doi:10.1038/s41561-023-01126-1.
- 662 Seidl, R., Thom, D., Kautz, M. et al. Forest disturbances under climate change. *Nature*
663 *Clim Change* 7, 395–402 (2017). <https://doi.org/10.1038/nclimate3303>
- 664 Seneviratne, S. I., Zhang, X., Adnan, M., Badi, W., Dereczynski, C., Di Luca, A., Ghosh,
665 S., Iskandar, I., Kossin, J., Lewis, S., Otto, F., Pinto, I., Satoh, M., Vicente-Serrano, S.
666 M., Wehner, M., and Zhou, B. (2021) Weather and Climate Extreme Events in a
667 Changing Climate, in: *Climate Change 2021: The Physical Science Basis. Contribution*
668 *of Working Group I to the Sixth Assessment Report of the Intergovernmental Panel on*
669 *Climate Change*, edited by: Masson-Delmotte, V., Zhai, P., Pirani, A., Connors, S. L.,
670 Péan, C., Berger, S., Caud, N., Chen, Y., Goldfarb, L., Gomis, M. I., Huang, M., Leitzell,
671 K., Lonnoy, E., Matthews, J. B. R., Maycock, T. K., Waterfield, T., Yelekçi, O., Yu, R.,
672 and Zhou, B., Cambridge University Press, Cambridge, United Kingdom and New York,
673 NY, USA, 1513–1766, <https://doi.org/10.1017/9781009157896.013>.
- 674 Shekhar, A., Hörtnagl, L., Buchmann, N., & Gharun, M. (2023). Long-term changes in
675 forest response to extreme atmospheric dryness. *Global Change Biology*, 29, 5379–
676 5396. <https://doi.org/10.1111/gcb.16846>

- 677 Shekhar A, Hörtnagl L, Paul-Limoges E, Etzold S, Zweifel R, Buchmann N, Gharun M
678 (2024a) Contrasting impact of extreme soil and atmospheric dryness on the functioning
679 of trees and forests. *Science of the Total Environment* 916, 169931.
680 <https://doi.org/10.1016/j.scitotenv.2024.169931>
- 681 Shekhar A, Humphrey V, Buchmann N, Gharun M (2024b). More than three-fold increase of
682 extreme dryness across Europe by end of 21st century. <https://doi.org/10.21203/rs.3.rs-3143908/v2> (under review in *Weather and Climate Extremes*)
- 684 Shekhar A, Buchmann N and Gharun M (2022) How well do recently reconstructed solar-
685 induced fluorescence datasets model gross primary productivity? *Remote Sens. Environ.* 283,
686 113282
- 687 Tripathy, K. P., & Mishra, A. K. (2023) How unusual is the 2022 European compound drought
688 and heatwave event? *Geophysical Research Letters*, 50, e2023GL105453.
689 <https://doi.org/10.1029/2023GL105453>
- 690 Tsakiris, G. and H. Vangelis, 2005. Establishing a Drought Index Incorporating
691 Evapotranspiration. *European Water* 9/10: 3-11.
- 692 van der Woude, A.M., Peters, W., Joetzjer, E. *et al.* Temperature extremes of 2022 reduced
693 carbon uptake by forests in Europe. *Nat Commun* 14, 6218 (2023).
694 <https://doi.org/10.1038/s41467-023-41851-0>
- 695 van der Molen MK, Dolman AJ, Ciais P et al (2011) Drought and ecosystem carbon cycling.
696 *Agric for Meteorol.* 151(7):765–773. <https://doi.org/10.1016/j.agrformet.2011.01.018>
- 697 Zhang J, Xiao J, Tong X, Zhang J, Meng P, Li J, Liu P, Yu P (2022) NIRv and SIF better estimate
698 phenology than NDVI and EVI: Effects of spring and autumn phenology on ecosystem
699 production of planted forests. *Agricultural and Forest Meteorology* 315, 108819
- 700 Zhou, S., Yu, B. and Zhang, Y. (2023). Global concurrent climate extremes exacerbated by
701 anthropogenic climate change. *Sci. Adv.* 9(10), p.eabo1638. doi:10.1126/sciadv.abo1638.
- 702 Wable PS, Jha MK, Shekhar A. Comparison of drought indices in a semi-Arid River basin of
703 India. *Water Resour Manag.* 2019;33:75–102. doi: 10.1007/s11269-018-2089-z
- 704 Wang B, Chen T, Xu G, Wu G, Liu G (2023) Management can mitigate drought legacy effects
705 on the growth of a moisture-sensitive conifer tree species. *Forest Ecology and Management*
706 544, 121196. <https://doi.org/10.1016/j.foreco.2023.121196>